The rotational excitation of the HCN and HNC molecules by H2 revisited

M. Hernández Vera, F. Lique, F. Dumouchel, Pierre Hily-Blant, A. Faure

Monthly Notices
of the
ROYAL ASTRONOMICAL SOCIETY

MNRAS **468,** 1084–1091 (2017)
Advance Access publication 2017 February 20

doi:10.1093/mnras/stx422

The rotational excitation of the HCN and HNC molecules by H_2 revisited

M. Hernández Vera,[1] F. Lique,[1⋆] F. Dumouchel,[1] P. Hily-Blant[2] and A. Faure[2]

[1]*LOMC - UMR 6294, CNRS-Universitdu Havre, 25 rue Philippe Lebon, BP 1123, F-76063 Le Havre, France*
[2]*UJF-Grenoble 1/CNRS, Institut de Planétologie et d'Astrophysique de Grenoble (IPAG) UMR 5274, F-38041 Grenoble, France*

Accepted 2017 February 16. Received 2017 February 10; in original form 2016 June 3

ABSTRACT

HCN and HNC are two fundamental molecules in the dense interstellar medium. The HNC/HCN abundance ratio depends on the kinetic temperature and can be used to explore the physical and chemical conditions of star-forming regions. Modelling of HCN and HNC emissions from interstellar clouds requires to model their collisional and radiative excitations. We report the calculation of the HCN and HNC excitation rate coefficients among the first 26 rotational levels due to H_2 collisions, for temperatures ranging from 5 to 500 K, using the exact close coupling and the approximate coupled states methods. We found a propensity for even Δj transitions in the case of HCN–para-H_2 collisions, whereas a propensity for odd Δj transitions is observed in the case of HNC–para-H_2 collisions. For collisions with ortho-H_2, both molecules show a propensity rule favouring transitions with odd Δj. The rate coefficients for HCN and HNC differ significantly, showing clearly that the collisional excitation of the two isomers is different, especially for para-H_2. We also evaluate the impact of these new data on the astrophysical modelling through radiative transfer calculations. It is shown that specific calculations have to be performed for the two isomers and that the HNC/HCN abundance ratio in cold molecular clouds cannot be estimated from line intensity ratio. Finally, observations of the two isotopologues $H^{13}CN$ and $HN^{13}C$ towards a sample of prestellar cores are presented, and the larger excitation temperature of $HN^{13}C$ is well reproduced by our excitation model.

Key words: molecular data – molecular processes – radiative transfer.

1 INTRODUCTION

Hydrogen cyanide and hydrogen isocyanide are the two fundamental and ubiquitous molecules in the interstellar medium (ISM). They have been detected towards diffuse clouds (Liszt & Lucas 2001), translucent molecular clouds (Turner, Pirogov & Minh 1997), dark clouds (Hirota et al. 1998), star-forming regions (Loughnane et al. 2012) and the circumstellar gas (Dutrey, Guilloteau & Guelin 1997; Kastner et al. 1997). HCN and HNC are considered as excellent tracers of high-density regions due their relatively large dipole moments, so that the critical density of the $j_1 = 1 \rightarrow 0$ transition (j_1 is the rotational quantum number of HCN or HNC) is as high as 10^6 cm^{-3}. Hence, they are used as star formation indicators, tracing dense molecular hydrogen gas within star-forming regions (Riechers et al. 2010).

Additionally, the HNC/HCN abundance ratio is known to strongly depend on the kinetic temperature (Schilke et al. 1992) and can be a useful tool to explore the physical and chemical conditions of star-forming regions. Indeed, extensive observations towards different evolutionary stages of massive star formation indicate that the HNC/HCN abundance ratio decreases with increasing temperature (e.g. Jin, Lee & Kim 2015, and references therein). The temperature dependence of the abundance ratio also suggests that it must be controlled by kinetics rather than thermodynamics (Herbst, Terzieva & Talbi 2000). In the nuclei of active galaxies, the HNC/HCN ratio is also employed to discriminate between photon-dominated regions and X-ray-dominated regions ((Meijerink, Spaans & Israel 2007)

Considering purely thermochemical considerations, the HNC/HCN abundance ratio should be almost zero in the cold molecular clouds since HNC is less stable than HCN by about $\simeq$7000 cm^{-1} (Bowman et al. 1993). Such hypothesis does not clearly hold in the ISM since the HNC/HCN abundance ratio increase with decreasing temperatures, the abundance of HNC being even larger than that of HCN in some cold media. Indeed, the HNC/HCN abundance ratio was found to vary from $\sim$1/100 in star-forming regions (Schilke et al. 1992), up to 4.5 in cold molecular clouds (Hirota et al. 1998). Such variations have still to be understood and remain a challenge for astrochemist, especially the HNC/HCN abundance ratio larger than 1 in cold molecular clouds.

In the ISM, the major source of both isomers is thought to be the dissociative recombination of $HCNH^+$ with electrons forming both HCN and HNC in equal measure (e.g. Mendes et al. 2012, and references therein). Several attempts have been done in order to explain the large variation of the observed HNC/HCN abundance

⋆ E-mail: francois.lique@univ-lehavre.fr

ratio. Recently, Graninger et al. (2014) used gas-phase model and a gas-grain model to simulate the formation of HCN and HNC in star-forming regions. These authors suggest that the only reaction that appears to be of importance in reducing the HNC/HCN ratio when the temperature increases is the reaction between HNC and atomic H. Loison, Wakelam & Hickson (2014) also found that the reaction of HCN with H_3^+ followed by the dissociative recombination of $HCNH^+$ acts to isomerize HCN into HNC leading to a HNC/HCN ratio close to or slightly lower than 1. Yet, despite the advances of the chemical models, the chemistry of these isomers is not fully understood and does not match with observations analysis.

In the absence of specific collisional data for the two isomers, the HNC/HCN abundance ratio was simply estimated from the line intensity ratio. However, due to the low density in the ISM, the energy levels of the interstellar molecules are generally out local thermodynamic equilibrium (LTE). Therefore, reliable determination of molecular abundances relies on radiative transfer calculations, which, in turn, require the knowledge of radiative and collisional data. Collisional data for the rotational excitation of HCN by He atoms (as a template for H_2) were provided first by Green & Thaddeus (1974) and Monteiro & Stutzki (1986) (see also references therein). During many years, in astrophysical applications, HNC and HCN were therefore assumed to present similar collisional rate coefficients (see in particular, the discussion in Guélin et al. 2007).

Recently, HCN and HNC molecules have been the object of new specific scattering studies. Sarrasin et al. (2010) studied the rotational excitation of HCN and HNC by collisions with He (as a model of para-H_2) obtaining differences larger than a factor of 5 for $\delta j_1 = 1$ transitions. This was the first evidence of different excitation mechanism for HCN and HNC. As a conclusion, these authors showed that the use of HCN rate coefficients to interpret HNC observations can lead to significant inaccuracies, in practice an overestimation of the HNC abundance. However, He is not the main collisional partner in the ISM. It may be used as a model of para-H_2 in some cases, but He and H_2 rate coefficients usually differ and the differences seen in HCN and HNC rate coefficients with the He collisional partner need to be confirmed with the dominant H_2 collisional partner.

Very recently, some of us have performed preliminary state-of-the-art calculations to study the rotational excitation of HCN and HNC by collisions with para-H_2 and ortho-H_2 (Dumouchel, Kłos & Lique 2011; Vera et al. 2014). In these papers, we improved the previous rate coefficients estimations by employing new highly correlated four dimensional (4D) potential energy surfaces (PESs) that considered the rotational structure of H_2.[1] These calculations suggest a similar conclusions to that of Sarrasin et al. (2010): The collisional rate coefficients of both isomers are significantly different, indicating that specific calculations must be performed to simulate their excitation in the ISM due to both He and H_2 collisional partners.

In the present paper, we extend the preliminary calculations of Vera et al. (2014) and Dumouchel et al. (2011) to the first 26 rotational levels (up to $j_1 = 25$) of both HCN and HNC and we analyse the effect of the new rate coefficients on the excitation of HCN and HNC for physical conditions representative of the cold ISM. The paper is organized as follows. Section 2 describes the scattering calculations for the HCN–H_2 and HNC–H_2 collisional systems. In Section 3.1, we perform radiative transfer calculations to simulate the molecular emissions of HCN and HNC we perform radiative transfer calculations to simulate the molecular emissions of HCN and HNC through a large velocity gradient (LVG) approach. Finally, in Section 3.2, we compare observational and theoretical excitation temperatures for the two isotopologues $H^{13}CN$ and $HN^{13}C$ in a sample of prestellar cores.

[1] Ben Abdallah et al. (2012) computed HCN–para-H_2 without considering the rotational structure of H_2. Vera et al. (2014) have shown that this approximation leads to important inaccuracies, particularly at low temperature.

2 SCATTERING CALCULATIONS

2.1 Potential energy surface

In our scattering calculations, we employed the recently computed HCN–H_2 PES of Denis-Alpizar et al. (2013) and HNC–H_2 PES of Dumouchel et al. (2011). We will briefly remind the features of the HCN–H_2 and HNC–H_2 PESs and we refer the reader to Denis-Alpizar et al. (2013) and Dumouchel et al. (2011) for more details.

For the HCN–H_2 interaction, the *ab initio* PES has been calculated using the explicitly correlated coupled cluster with single, double and perturbative triple excitations [CCSD(T)-F12a] (Adler, Knizia & Werner 2007; Knizia, Adler & Werner 2009) method with an augmented correlation-consistent triple zeta (aug-cc-pVTZ) basis set (Dunning 1989). Both molecules were treated as rigid rotors. The equilibrium structure is linear with the nitrogen of HCN pointing towards H_2 at an intermolecular separation of 7.20 a_0. The corresponding well depth is -195.20 cm^{-1}. A secondary minimum of -183.59 cm^{-1} was found for a T-shape configuration with the H of HCN pointing towards the centre of mass of H_2. Then, in order to solve the close-coupling equations for scattering, the PES was expanded over angular functions for all R distances (Green 1975): The accuracy of this new PES was estimated by comparing theoretical HCN–H_2 transition frequencies with the experimental ones of Ishiguro et al. (2001, 2012). The agreement between the theoretical and experimental results was found to be better than 0.5 per cent showing that the PES can be used with confidence for the scattering calculations.

Ab initio calculations of the HNC–H_2 PES were carried out at the coupled cluster with single, double and perturbative triple excitations (CCSD(T); Hampel, Peterson & Werner 1992; Watts, Gauss & Bartlett 1993) level of theory. The calculations were performed with the aug-cc-pVTZ basis set augmented with bond functions defined by Williams et al. (1995). The PES was also expanded over angular functions using the expression of Green (1975). The global minimum of 309.64 cm^{-1} of the PES occurs for a T-shaped structure with HNC being the stem of the T letter. The equilibrium distance is 6.9 a_0, the geometry corresponds to HNC pointing with its H-end towards the bond of the H_2 molecule.

Both HCN–H_2 and HNC–H_2 PESs have similar accuracy and the difference seen in the collisional data cannot be due to the slightly different methods used in the *ab initio* calculations.

2.2 Dynamical calculations

In this paper, we investigate the following inelastic collision processes:

$$\mathrm{HCN}(j_1) + \mathrm{o;p{-}H_2}(j_2) \rightarrow \mathrm{HCN}(j_1') + \mathrm{o;p{-}H_2}(j_2') \quad (1)$$

$$\mathrm{HNC}(j_1) + \mathrm{o;p{-}H_2}(j_2) \rightarrow \mathrm{HNC}(j_1') + \mathrm{o;p{-}H_2}(j_2'), \quad (2)$$

where j_1 and j_2 represent the rotational energy levels of HCN (HNC) and H_2, respectively. p-H_2 and o-H_2 designate para-H_2 and

Table 1. Close coupling and coupled-states rate coefficients for the HNC and HCN molecules in collision with para-H_2($j_2 = 0$) (in unit of $\times 10^{-11}$ cm^3 molecule^{-1} s^{-1}).

		HNC		HCN	
$j_1 - j_1'$	T(K)	CC	CS	CC	CS
1 − 0	50	10.1	9.43	2.23	4.48
	100	10.3	9.60	2.22	4.16
2 − 1	50	15.9	14.8	3.16	6.03
	100	14.9	14.4	3.23	5.89
5 − 3	50	9.44	9.21	9.49	7.25
	100	9.47	9.76	11.1	9.33
5 − 4	50	18.3	17.7	3.89	2.45
	100	18.2	17.2	3.99	3.23
8 − 3	50	0.76	0.53	0.13	0.10
	100	0.94	0.73	0.25	0.22

ortho-H_2. Note that the para–ortho-H_2 conversion is forbidden during the collisions. The hyperfine structure of the HCN and HNC molecules is neglected in these calculations, but can be considered through from the present data using recoupling techniques as presented in Lanza & Lique (2014).

We use of the 4-dimensional HCN–H_2 and HNC–H_2 PES to determine rotational excitation and de-excitation cross-sections between the first 26 rotational levels of HCN and HNC. The rotational levels of HCN, HNC and H_2 were obtained using the experimental spectroscopic constants from Huber & Herzberg (1979).

Close coupling (CC) approach (Green 1975) is computationally challenging for such heavy molecules. Hence, we have also used the coupled-states approximation (CS; McGuire & Kouri 1974) to compute the excitation cross-sections. The validity of the CS approach is presented in Table 1.

For HNC, it has been found that the CS approach can lead to inaccuracies of 20–30 per cent for very low temperature rate coefficients (<50 K) and for transitions with large Δj_1. However, a good agreement exists between CC and CS rate coefficients when the temperature is greater than 50 K. For HCN, the global agreement between CC and CS results is good despite the difference can be as large as a factor of 2 for transitions involving the lowest rotations levels. As a consequence, for transitions between the first rotational states of HCN and HNC, we decided to also extend the CC results to higher temperatures. Hence, the rate coefficients between the first 11 and 13 levels of HNC and HCN molecules, respectively, were obtained using a pure CC approach up to 500 K. Note that HCN and HNC rate coefficients at low temperatures are identical to that of Vera et al. (2014) and Dumouchel et al. (2011), respectively.

The standard time-independent coupled scattering equations were solved using the MOLSCAT code Hutson & Green (1994). Calculations were performed for total energy up to 3500 cm^{-1} for collision of HCN and HNC with both para-H_2 and ortho-H_2. The integration parameters were selected to ensure convergence of the cross-sections over all the energy range. Generally, the integration range extended from 4 to 50 a_0 and the STEPS parameter allows to constrain the step length of the integrator below 0.1 to 0.2 a_0. The HCN and HNC rotational basis was sufficiently extended to ensure convergence of the inelastic cross-sections. At the largest total energy considered ($E = 3500$ cm^{-1}) the HCN rotational basis was extended to $j_1 = 35$ to ensure convergence of the first 26 (up to $j_1 = 25$) rotational levels and the HNC rotational basis was extended to $j_1 = 32$ to also ensure convergence of the first 26 (up to $j_1 = 25$) rotational levels. The rotational basis of H_2 included levels up to $j_2 = 2$. The maximum value of the total angular momentum J used in the calculations was set large enough ($J_{max} = 142$ for HCN and $J_{max} = 135$ for HNC at $E = 3500$ cm^{-1}) so that the inelastic cross-sections were converged to within 0.05 Å^2.

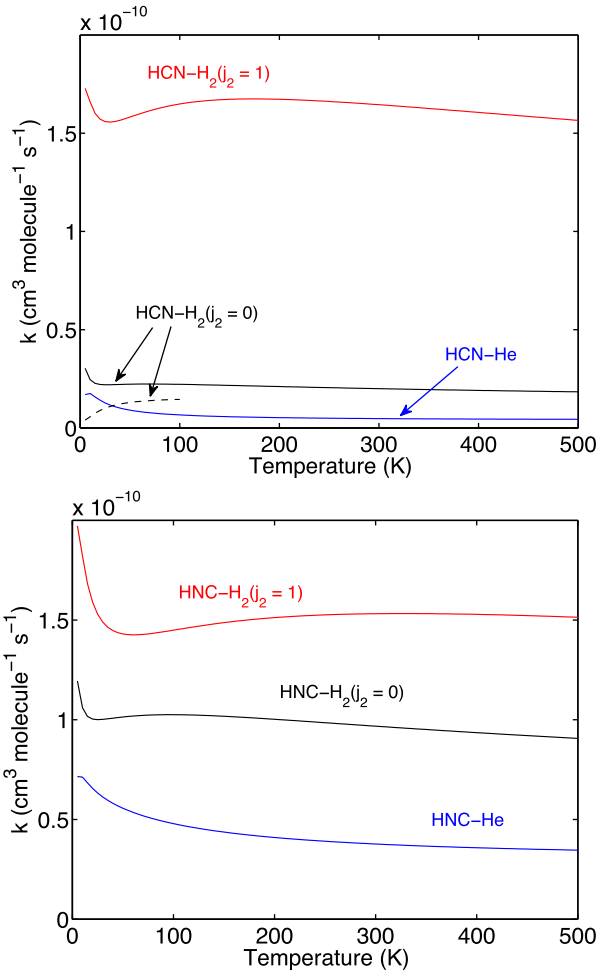

Figure 1. Upper panel: Temperature variation of the HCN–H_2 (both para- and ortho-H_2) and HCN–He rate coefficients for the $j_1 = 1 - 0$ transitions. The dashed line corresponds to the results of Ben Abdallah et al. (2012). Lower panel: Temperature variation of the HNC–H_2 (both para- and ortho-H_2) and HNC–He rate coefficients for the $j_1 = 1 - 0$ transitions.

From the inelastic cross-sections $\sigma_{j_1 j_2 \to j_1' j_2'}(E_c)$, we have obtained the corresponding thermal rate coefficients at temperature T by a boltzmann average over the collision energy (E_c):

$$k_{j_1 j_2 \to j_1' j_2'}(T) = \left(\frac{8}{\pi \mu k^3 T^3}\right)^{1/2} \times \int_0^\infty \sigma_{j_1 j_2 \to j_1' j_2'} E_c \, e^{-E_c/k_B T} \, dE_c, \quad (3)$$

where k_B is the Boltzmann's constant. Calculations up to the total energy of 3500 cm^{-1} allow us to determine rate coefficients up to 500 K. The complete set of (de-)excitation rate coefficients will be made available through the Leiden Atomic and Molecular Database (Schöier et al. 2005) and BASECOL (Dubernet et al. 2013) data bases.

2.3 Results

Fig. 1 shows, the temperature dependence of the $j_1 = 1 - 0$ de-excitation rate coefficients of HCN and HNC in collision with

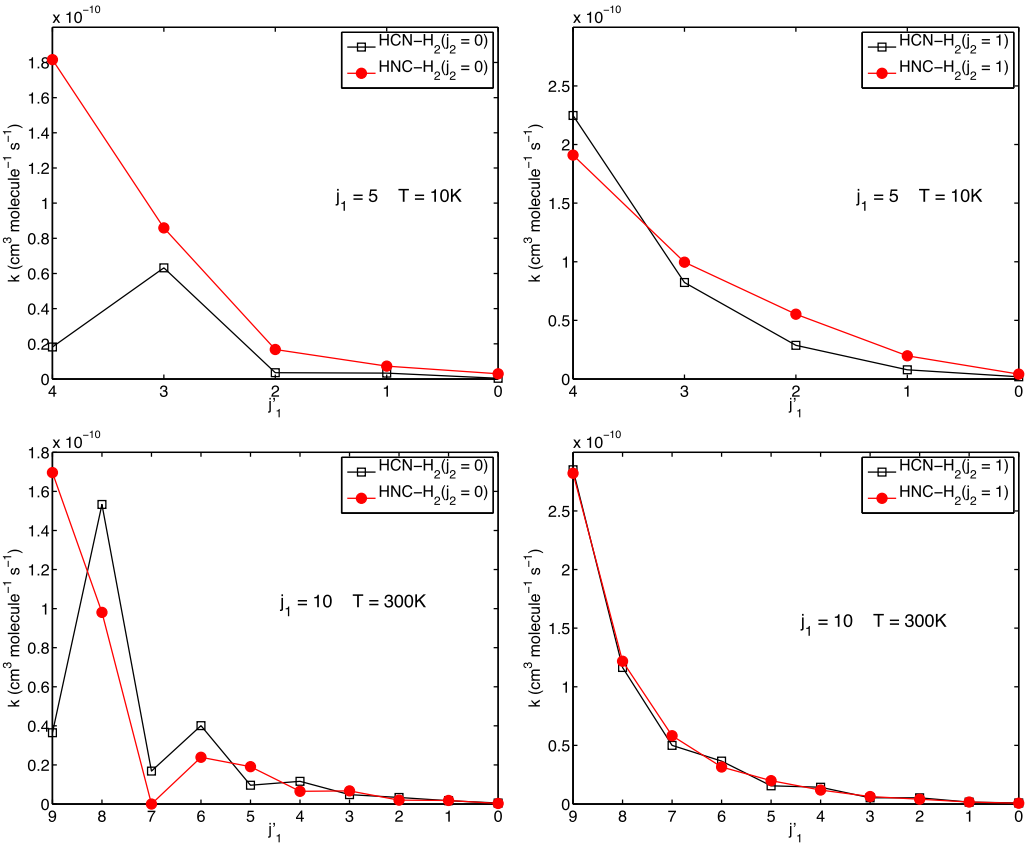

Figure 2. HCN–H_2 and HNC–H_2 de-excitation rate coefficients from the initial level $j_1 = 5$ at 10 K (upper panels) and from the initial level $j_1 = 10$ at 300 K (lower panels).

para-H_2($j_2 = 0$) and ortho-H_2($j_2 = 1$). We also show on this plot the de-excitation rate coefficients of HCN and HNC in collisions with He of Dumouchel, Faure & Lique (2010) and with para-H_2($j_2 = 0$) of Ben Abdallah et al. (2012).

First, we found differences between collisions with the two H_2 species. The rate coefficients for collisions with H_2($j_2 = 1$) are up to two-to-three times larger than that of H_2($j_2 = 0$), especially for HCN. We also note important deviations between He and H_2 rate coefficients, particularly with the ortho-H_2 rate coefficients, where He and ortho-H_2 rate coefficients can differ up to an order of magnitude. Finally, we also note significant difference between the present rate coefficients and that of Ben Abdallah et al. (2012). Such differences were already discussed by Vera et al. (2014) and were a consequence of the reduced dimension approach used by Ben Abdallah et al. (2012) to describe the collisional process.

We are also interested in the propensity rules of HCN and HNC rotational transitions due to H_2 collisions. Fig. 2 presents downward rotational rate coefficients out of HCN (HNC)($j_1 = 5$ and 10) levels at 10 and 300 K.

It is interesting to note that for collisions with para-H_2, HCN rate coefficients with $\Delta j_1 = 2$ are larger than those with $\Delta j_1 = 1$, while the reverse applies for HNC. For collisions with ortho-H_2, a propensity rules in favour of $\Delta j_1 = 1$ is found for both molecules. Hence, the propensity depends on the quantum state of the hydrogen molecule. For collisions with para-H_2, we found that the differences between HCN and HNC rate coefficients can be up to an order of magnitude for the $\Delta j_1 = 1$ transitions, the differences between HCN and HNC rate coefficients being more pronounced at low temperatures than at high temperatures. Such comparison confirms the different excitation of the two isomers, which was found by Dumouchel et al. (2010) when using the He collisional partner. This could have a strong influence on the HNC/HCN abundance ratio derived from the observations since the derived abundance of both molecules in space will be significantly dependent on the rate coefficients. For collisions with ortho-H_2, the difference between HCN and HNC rate coefficients are very moderate. It shows that the excitation of the two isomers will be similar in warm ISM, where the ortho-H_2 collisional partner will be dominant.

3 ASTROPHYSICAL APPLICATIONS

3.1 The excitation of HCN and HNC

The comparison of both sets of rate coefficients indicates clearly that the excitation of HCN and HNC is different, especially due to para-H_2. In order to evaluate the impact of the new collisional data on the astrophysical modelling, we have simulated the excitation of both HCN and HNC in cold molecular clouds. The escape probability formalism was employed with the publicly available RADEX code (van der Tak et al. 2007). In this approximation, the code refers to an expanding spherical shell. As a background radiation field, we included the 2.7 K cosmic microwave background only. The computation depends on a few basic parameters: The density of the collider (here both para- and ortho-H_2), the kinetic temperature (T), the total column density (N) of HCN and HNC and Δv the full width at half-maximum of the lines, which was held fixed at 1 km s^{-1}. In the following, the kinetic temperature was fixed at 10 and 30 K, and the H_2 density has been varied from n_{H_2}= 10^2 to 10^9 cm^{-3}.

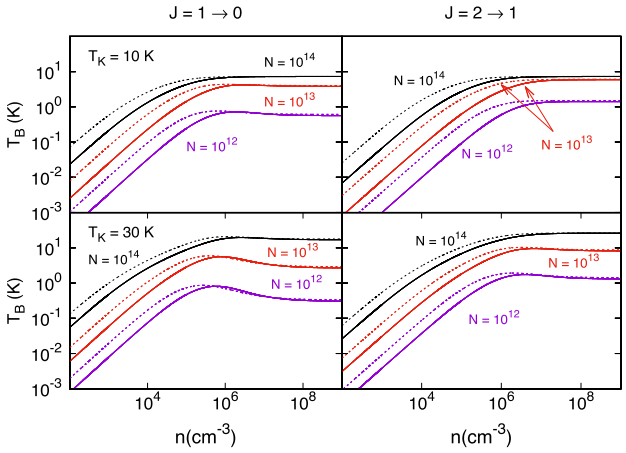

Figure 3. Solid lines: brightness temperature for the $j_1 = 1 - 0$ and $j_1 = 2 - 1$ lines of HCN (indicated at the top of each column) derived using our new rate coefficients for temperatures of 10 and 30 K (indicated in the left-hand panels). The column density takes the values 10^{12}, 10^{13} and 10^{14} cm^{-2}. Brightness temperatures are in K and densities in cm^{-3}. Dashed lines: the same for HNC.

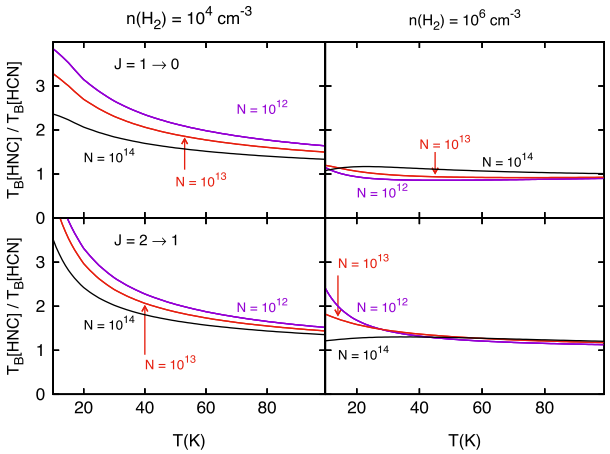

Figure 4. The intensity ratio of the $j_1 = 1 - 0$ and $j_1 = 2 - 1$ lines (as indicated in the left-hand panels) using our collisional HCN–H_2 and HNC–H_2 rate coefficients. Two hydrogen densities, $n_{H_2} = 10^4$ and 10^6 cm^{-3}, have been considered as indicated in the top panels. We also considered three cases for the opacity of the $j_1 = 1 - 0$ line: optically thin ($N = 10^{12}$ cm^{-2}) moderately thick $\tau \simeq 1$, ($N = 10^{13}$) and optically thick ($N = 10^{14}$ cm^{-2}). The kinetic temperature varies between 10 and 100 K.

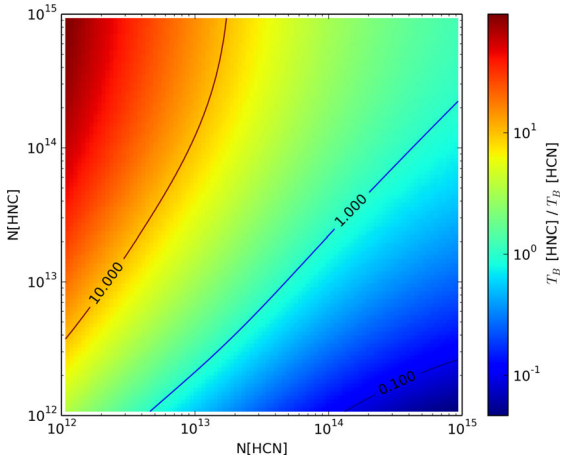

Figure 5. Color scale map of the HNC/HCN brightness temperature ratio for the $j_1 = 1 - 0$ transition. In the calculations, hydrogen density was fixed at n(H_2) = 3×10^4 cm^{-3} and the kinetic temperature was fixed at 10 K.

The column densities of both HCN and HNC were taken at 10^{12}, 10^{13} and 10^{14} cm^{-2}. We assume a thermal Boltzmann distribution of the two H_2 nuclear spin isomers. Boltzmann averaging was done using partition function of the first three rotational states of the H_2 molecule. In molecular clouds, the para–ortho-H_2 abundance ratio frequently deviates from a thermal Boltzmann distribution and it will be possible to use in molecular emission modelling, a different para–ortho-H_2 abundance ratio since collisional rate coefficients will be provided at a state-to-state level. The first 11 rotational levels of HCN and HNC were included in the calculations.

In Fig. 3, we show the brightness temperatures of the $j_1 = 1 - 0$ and $j_1 = 2 - 1$ lines for both HCN and HNC molecules. For molecular hydrogen densities lower than 10^6 cm^{-3}, the differences between the $j_1 = 1 - 0$ and $j_1 = 2 - 1$ brightness temperatures of HCN and HNC are large. In contrast, at densities higher than 10^6 cm^{-3}, when LTE conditions are reached, the brightness temperatures of both isomers do not differ much because of their similar dipole moments and rotational constants.

The differences between HCN and HNC emission can be clearly shown by plotting the ratio of the line intensity of both isomers, and assuming equal column densities for both species. Fig. 4 shows the predicted line intensity ratio of the $j_1 = 1 - 0$ and $j_1 = 2 - 1$ lines, as a function of the kinetic temperature, while the H_2 density was fixed to either $n_{H_2} = 10^4$ or 10^6 cm^{-3}. The column densities of HCN and HNC were equal and set at 10^{12}, 10^{13} and 10^{14} cm^{-2}. As can be seen, the line ratios decrease with increasing the kinetic temperature, approaching unity for temperatures around 100 K, whatever the column densities are. However, for low and moderate kinetic temperature there are significant differences between HCN and HNC brightness temperatures. At low densities, the $j_1 = 1 - 0$ transition of HNC are predicted up to a factor of 4 stronger than the $j_1 = 1 - 0$ transition of HCN, while in the case of $j_1 = 2 - 1$ transitions, the differences reach a factor of 5. The line intensity ratios reach their maximum difference in the optically thin regime, as expected. At higher hydrogen densities, the line intensity of both isomers is pretty similar since we approach the LTE.

In Fig. 5, we further explore the effects of our new rate coefficients on the predicted line intensities of HCN and HNC. The figure maps the HNC/HCN $j_1 = 1 - 0$ line intensity ratio as a function of the column densities of HCN and HNC. We fixed the hydrogen density to 3×10^4 cm^{-3} and the kinetic temperature to 10 K, which are typical physical conditions in dark molecular clouds (Bergin & Tafalla 2007). The column densities of HCN and HNC vary from 10^{12} to 10^{15} cm^{-2}. As we can see on this map, a line ratio of one does not corresponds to equal abundances of each isomer. Instead, equal line intensities are obtained for an HNC/HCN abundance ratio of ≈0.2. Conversely, assuming equal abundances, the HNC $j_1 = 1 - 0$ line will be stronger than the HCN one, i.e. it is more easily excited which is a direct result of the larger collisional rate coefficients for HNC.

3.2 Comparison with H^{13}CN and HN^{13}C towards prestellar cores

In cold prestellar cores, HCN and HNC isomers essentially result from the dissociative recombination of $HCNH^+$, with nearly equal branching ratios (Mendes et al. 2012). Their gas-phase abundances are thus expected to be equal. However, observations indicate

HNC/HCN abundance ratios within factors of a few both above and below unity (Hirota et al. 1998), raising the question whether such deviations reflect genuine chemical processes or radiative transfer effects. Using the rotational rate coefficients for the HCN–He et HNC–He collisional systems of Dumouchel et al. (2010), Padovani et al. (2011) found a good agreement between the predicted excitation temperatures (T_{ex}) with those derived from hyperfine spectra of $H^{13}CN$ and $HN^{13}C$ under the single-T_{ex} assumption for all hyperfine components of both species. We are here interested chiefly on deriving constraints on the $HN^{13}C/H^{13}CN$ abundance ratio X, from the excitation temperature and opacity of observed $j_1 = 1 - 0$ lines of each species.

We have performed new observations of the $H^{13}CN$ and $HN^{13}C$ $j_1 = 1 - 0$ rotational lines towards a sample of starless prestellar cores. The data, which will be presented into more details in a forthcoming paper, include and significantly extend the sample of Padovani et al. (2011). The basic properties of the sources are summarized in Table 2. The observations were done with the IRAM-30m

Table 2. Summary of the observations.

Source	RA(2000)	Dec.(2000)	Velocity[(1)] ($km\,s^{-1}$)	$1\sigma(H^{13}CN)$[(2)] (mK)	$1\sigma(HN^{13}C)$[(2)] (mK)
L1495BA	04:18:05.1	28:22:22.0	6.80	18	59
L1498[a]	04:10:51.5	25:09:58.0	7.80	36	33
L1507A	04:42:38.6	29:43:45.0	6.20	7	24
L1521B	04:24:12.7	26:36:53.0	6.44	11	24
L1521E[a]	04:29:15.7	26:14:05.0	6.90	21	
L1544	05:04:16.9	25:10:47.0	7.20	10	23
TMC2[a]	04:32:48.7	24:25:12.0	6.20	22	29
L183	15:54:08.8	−02:52:44.0	2.37	9	16

Notes. (1) LSR velocity.
(2) rms of the averaged spectra, in main-beam temperature scale.
[a]From Padovani et al. (2011).

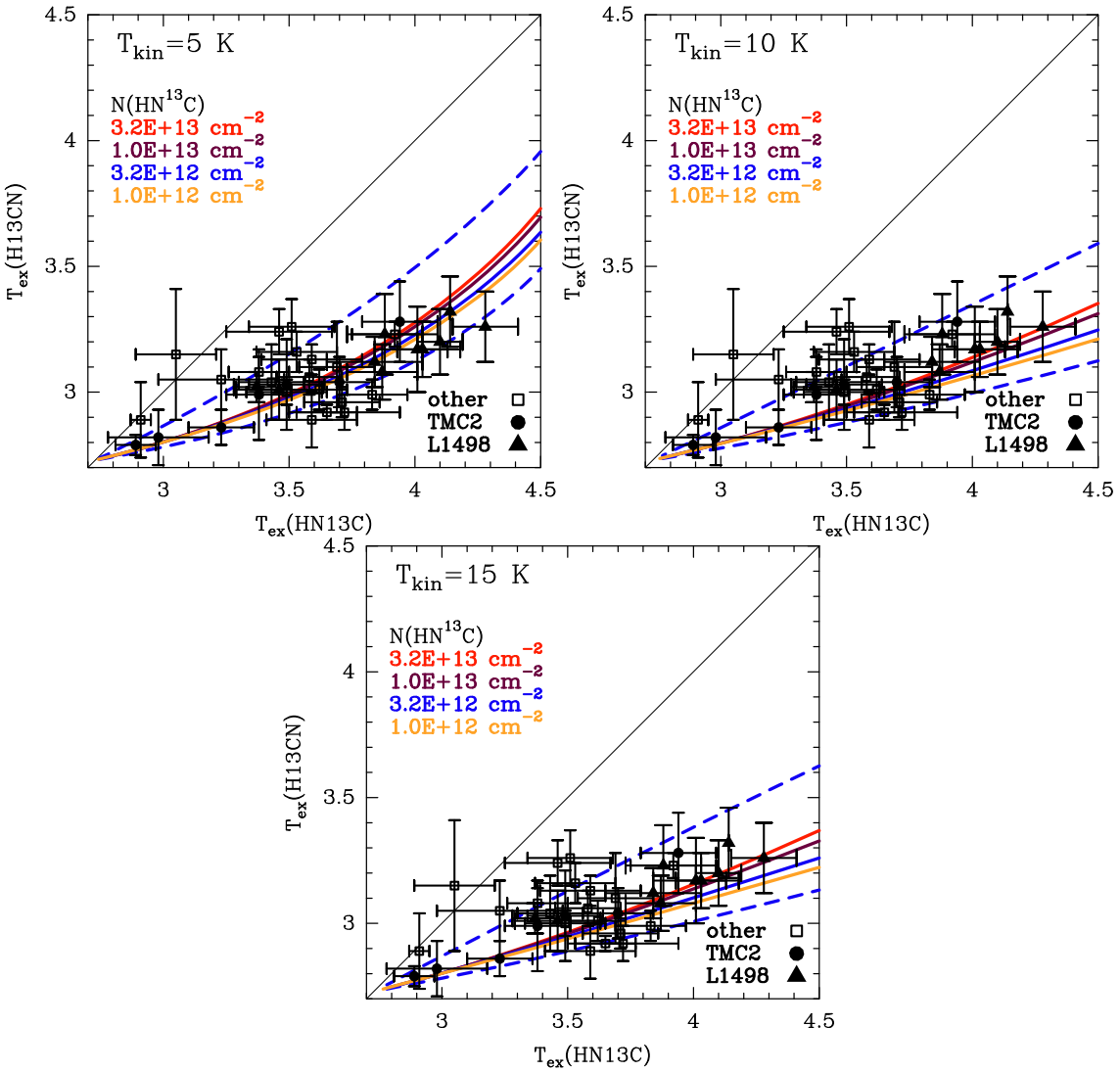

Figure 6. The $H^{13}CN$ and $HN^{13}C$ excitation temperatures towards a sample of prestellar cores derived from their $j_1 = 1 - 0$ rotational spectra (see Table 2) are compared to predictions (see Section 3.2) from radiative transfer calculations in the escape probability formalism. Each panel shows the results at a given kinetic temperatures (5, 10 and 15 K), while covering a range in the $HN^{13}C$ column density (0.1 to 3.2×10^{13} cm^{-2}, full curves) and an equal column density of $H^{13}CN$, and varying also the H_2 density (10^3 to 10^6 cm^{-3}). To indicate the influence of the $HN^{13}C/H^{13}CN$ ratio, results for ratios of 0.3 (top) and 3 (bottom) are also shown (dashed blue curves).

telescope, using the EMIR receivers (Carter et al. 2012) in combination with the VESPA providing spectral resolutions of 20 kHz or 0.07 km s^{-1}. The receivers were tuned at 86 340.184 MHz for H^{13}CN and 87 090.825 MHz for HN^{13}C.

The hyperfine structure of the H^{13}CN $j_1 = 1 - 0$ is easily resolved, while that of the HN^{13}C is only partially. For the latter, we used the prescription described in van der Tak et al. (2009) and summarized in Padovani et al. (2011). To derive the excitation temperature and opacity of both lines, we assumed equal excitation temperatures for all hyperfine components and applied the hyperfine structure routine of the CLASS software. Towards each source and offset position, we derived the rotational opacity and excitation temperature of each $j_1 = 1 - 0$ line. The results are shown in Fig. 6. As can be seen, the excitation temperature of H^{13}CN $j_1 = 1 - 0$ is smaller than that of HN^{13}C $j_1 = 1 - 0$, with only a few exceptions. The associated rotational opacities (Fig. 7) are between 1 and 10, and are similar for both species.

We have compared the observed excitation temperature with the predictions from non-LTE calculations in the escape probability formalism (with the RADEX code) and using our new rotational rate coefficients. The collisional rate coefficients for H^{13}CN and HN^{13}C were assumed identical to those of HCN and HNC, respectively. Indeed, mass effects between ^{12}C and ^{13}C are almost negligible in the scattering. However, isotopologue-specific energy levels and radiative rates were correctly selected. In performing the non-LTE calculations, we varied the density of collisioners, n_{H_2}, between 10^3 and 10^6 cm^{-3}, while the kinetic temperature T_{kin} covers the range of 5 to 20 K. The column density of H^{13}CN and HN^{13}C encompass the typical values of prestellar cores (Hily-Blant et al. 2010; Padovani et al. 2011), from 0.1 to 10 $\times$ 10^{13} cm^{-2}. For each HN^{13}C column density, the abundance ratio X = HN^{13}C/H^{13}CN was varied from 0.3 to 10. Results are shown in Fig. 6 at three kinetic temperatures, showing the overall agreement with the observations. At 10 K, the improvement with respect to Padovani et al. (2011) is ascribed to the use of our new collisional rate coefficients. The agreement deteriorates at higher temperatures, while it improves at kinetic temperatures lower than 10 K, in harmony with ammonia observations towards prestellar cores (Crapsi et al. 2007). The improvement is especially visible for TMC2 and L1498. To evince the influence of the abundance ratio, predictions are also shown for $X = 0.3$ and 3, and it can be seen that this range covers much of the observed cores and positions. However, a single set of column density and abundance ratio X does not reflect the ensemble of observed spectra, suggesting measurable source-to-source variation. In particular, it is not possible with our simplified analysis, to determine separately the physical conditions and column density from the excitation temperature only.

Further constraints can, however, be obtained from the rotational opacity of H^{13}CN and HN^{13}C, as summarized in Fig. 7. At a temperature of 5 K, the best agreement is obtained for a HN^{13}C column density of 10^{13} cm^{-2}, an H_2 density lower than 10^5 cm^{-3}, and an abundance ratio between $X = 1$ and 3, or H^{13}CN column densities of 0.3–1 $\times$ 10^{13} cm^{-2}. At a higher temperature of 10 K, the previous solutions again fit very well the observations but only for H_2 densities lower than $\sim 10^4$ cm^{-3}. A larger column density of HN^{13}C [N(HN^{13}C) = 3.2 $\times$ 10^{13} cm^{-2}], and moderately larger density (10^5 cm^{-3}) are also compatible with the observed opacities while keeping the H^{13}CN column density unchanged, namely 0.3–1 $\times$ 10^{13} cm^{-2}. The higher density reflects the increased population of higher j_1 levels. In all cases, the HN^{13}C / H^{13}CN abundance ratio is constrained to values $X = 1$ to 3. This result can presumably not be ascribed to a differential sensitivity of HCN and HNC to carbon fractionation (Roueff, Loison & Hickson 2015), and may thus reflect the HNC/HCN abundance ratio. If this is the case, an efficient HCN $\rightarrow$ HNC isomerization mechanism must occur in prestellar cores. An alternative explanation would be radiative transfer effects (e.g. deviations from a single-excitation temperature within the hyperfine levels), which our simplified analysis does not take into account. We anticipate that deviations from the single-T_{ex} assumption are likely small because of the moderate opacity of the H^{13}CN and HN^{13}C lines (Daniel & Cernicharo 2008). To firmly disentangle between a chemical or a radiative transfer origin for the observed HNC/HCN ratio requires thorough calculations using collisional rates at the hyperfine level together with state-of-the art radiative transfer taking into account hyperfine overlap and a physical source structure (Daniel et al. 2016), which are beyond the scope of the paper.

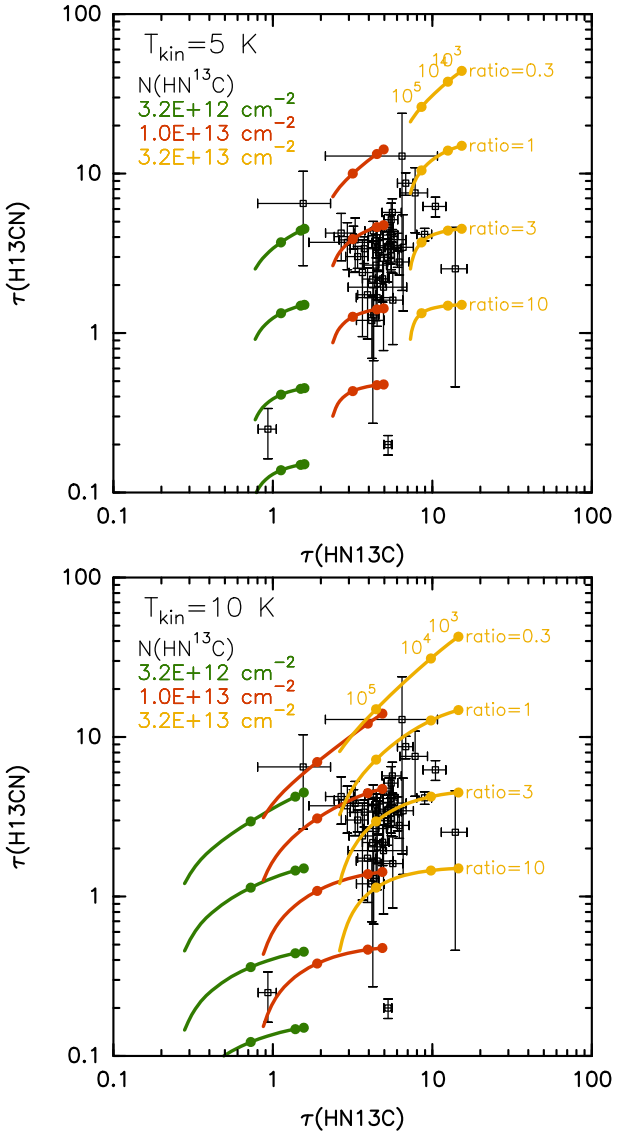

Figure 7. The predicted opacity, from the same set of models of Fig. 6, are compared to the observed ones (shown here for at T_{kin} = 5 and 10 K). The density along each curve is also indicated.

4 CONCLUSION

We have used quantum scattering calculations to investigate the rotational energy transfer in collisions of HCN and HNC molecules with H_2 molecules. The calculations are based on recent, highly accurate 4D PESs. Rate coefficients for transitions involving the lowest 26 levels of these molecules were determined for temperatures ranging from 10 to 500 K. Strong propensity rules for even Δj_1 were found in the case of HCN–para-H_2 system, whereas propensity rules for odd Δj_1 were found in the case of HNC–para-H_2 system. The excitation of HCN and HNC molecules in the cold ISM is then confirmed to be very different and put in evidence the need of specific observations analysis for the two isomers. Indeed, the new observations confirm the different excitations of the two isomers, while the new rates improve the agreement between model and observations. A simple analysis of the excitation conditions suggests kinetic temperatures lower than 10 K and $H^{13}NC/H^{13}CN$ abundance ratios in the range of 1–3. Finally, we plan to extend the present calculations to consider the hyperfine structure of the molecule in order to provide the astrophysical community with all the collisional tools to accurately model the observations of both HCN and HNC.

ACKNOWLEDGEMENTS

This research was supported by the CNRS national program 'Physique et Chimie du Milieu Interstellaire'. MHV and FL acknowledge the french embassy of Cuba and Campus France for financial support. PHB acknowledges the Institut Universitaire de France for financial support.

REFERENCES

Adler T. B., Knizia G., Werner H.-J., 2007, J. Chem. Phys., 127, 221106
Ben Abdallah D., Najar F., Jaidane N., Dumouchel F., Lique F., 2012, MNRAS, 419, 2441
Bergin E. A., Tafalla M., 2007, Annual Rev. A&A, 45, 339
Bowman J. M., Gazdy B., Bentley J. A., Lee T. J., Dateo C. E., 1993, J. Chem. Phys., 99, 308
Carter M. et al., 2012, A&A, 538, A89
Crapsi A., Caselli P., Walmsley M. C., Tafalla M., 2007, A&A, 470, 221
Daniel F., Cernicharo J., 2008, A&A, 488, 1237
Daniel F. et al., 2016, A&A, 592, A45
Denis-Alpizar O., Kalugina Y., Stoecklin T., Vera M. H., Lique F., 2013, J. Chem. Phys., 224301, 139
Dubernet M.-L. et al., 2013, A&A, 553, A50
Dumouchel F., Faure A., Lique F., 2010, MNRAS, 406, 2488
Dumouchel F., Kłos J., Lique F., 2011, Phys. Chem. Chem. Phys., 13, 8204
Dunning T. H., 1989, J. Chem. Phys., 90, 1007
Dutrey A., Guilloteau S., Guelin M., 1997, A&A, 317, L55
Graninger D. M., Herbst E., Öberg K. I., Vasyunin A. I., 2014, ApJ, 787, 74
Green S., 1975, J. Chem. Phys., 62, 2271
Green S., Thaddeus P., 1974, ApJ, 191, 653
Guélin M. et al., 2007, A&A, 462, L45
Hampel C., Peterson K. A., Werner H.-J., 1992, Chem. Phys. Lett., 190, 1
Herbst E., Terzieva R., Talbi D., 2000, MNRAS, 311, 869
Hily-Blant P., Walmsley M., Pineau des Forêts G., Flower D., 2010, A&A, 513, A41
Hirota T., Yamamoto S., Mikami H., Ohishi M., 1998, ApJ, 503, 717
Huber K. P., Herzberg G., 1979, Molecular Spectra and Molecular Structure. IV. Constants of Diatomic Molecules. Van Nostrand Reinhold, New York
Hutson J. M., Green S., 1994, Distributed by Collaborative Computational Project No. 6. Engin., Phys. Sci. Res. Council, Swindon
Ishiguro M., Tanaka T., Harada K., Whitham C. J., Tanaka K., 2001, J. Chem. Phys., 5137, 115
Ishiguro M., Harada K., Tanaka K., Tanaka T., Sumiyoshi Y., Endo Y., 2012, J. Chem. Phys., 33, 554
Jin M., Lee J.-E., Kim K.-T., 2015, ApJ, 219, 2
Kastner J. H., Zuckerman B., Weintraub D. A., Forveille T., 1997, Science, 277, 67
Knizia G., Adler T. B., Werner H.-J., 2009, J. Chem. Phys., 130, 054104
Lanza M., Lique F., 2014, J. Chem. Phys., 141, 164321
Liszt H., Lucas R., 2001, A&A, 370, 576
Loison J.-C., Wakelam V., Hickson K. M., 2014, MNRAS, 443, 398
Loughnane R. M., Redman M. P., Thompson M. A., Lo N., O'Dwyer B., Cunningham M. R., 2012, MNRAS, 420, 1367
McGuire P., Kouri D. J., 1974, J. Chem. Phys., 60, 463
Meijerink R., Spaans M., Israel F. P., 2007, A&A, 461, 793
Mendes M. B. et al., 2012, ApJ, 746, L8
Monteiro T. S., Stutzki J., 1986, MNRAS, 221, 33P
Padovani M., Walmsley C. M., Tafalla M., Hily-Blant P., Pineau des Forêts G., 2011, A&A, 534, A77
Riechers D. A., Weiß A., Walter F., Wagg J., 2010, ApJ, 725, 1032
Roueff E., Loison J. C., Hickson K. M., 2015, A&A, 576, A99
Sarrasin E., Abdallah D. B., Wernli M., Faure A., Cernicharo J., Lique F., 2010, MNRAS, 404, 518
Schilke P., Walmsley C. M., Pineau Des Forets G., Roueff E., Flower D. R., Guilloteau S., 1992, A&A, 256, 595
Schöier F. L., van der Tak F. F. S., van Dishoeck E. F., Black J. H., 2005, A&A, 432, 369
Turner B. E., Pirogov L., Minh Y. C., 1997, ApJ, 483, 235
van der Tak F. F. S., Black J. H., Schöier F. L., Jansen D. J., van Dishoeck E. F., 2007, A&A, 468, 627
van der Tak F. F. S., Müller H. S. P., Harding M. E., Gauss J., 2009, A&A, 507, 347
Vera M. H., Kalugina Y., Denis-Apizar O., Stoecklin T., Lique F., 2014, J. Chem. Phys., 140, 224302
Watts J. D., Gauss J., Bartlett R. J., 1993, J. Chem. Phys., 98, 8718
Williams H. L., Mass E. M., Szalewicz K., Jeziorski B., 1995, J. Chem. Phys., 103, 7374

This paper has been typeset from a TEX/LATEX file prepared by the author.